

Effect of Guest Size on the Mechanical Properties and Molecular Structure of Gas Hydrates from First-Principles

Thomas M. Vlastic, Phillip D. Servio, Alejandro D. Rey*

Department of Chemical Engineering, McGill University, Montréal, QC, H3A 0C5

Abstract

The elastic and acoustic properties of several sII gas hydrates with hydrocarbon guests (methane, ethane, propane, and isobutane) were investigated and quantified using density functional theory. The shear modulus of ethane-methane hydrates was found to be the highest among all investigated hydrates. Simple (single-guest) hydrates were found to be less resistant to shear stresses than mixed (double-guest) hydrates. In fact, the shear properties (i.e. shear modulus and shear wave velocity) were shown to be closely related to the level of anisotropy in the hydrate crystal lattice, which itself was a function of guest size. A linearly decreasing relationship between the compressional wave velocity and the molecular weight of the guest was also presented. The hydrate crystal structure was analyzed at the atomistic level during triaxial compression and extension. The main findings were that the ultimate tensile strength decreases with guest size, the large cages are more compressible than the small cages, and the bond lengths (H-bonds and O-H bonds) exhibit opposite behaviour (i.e. when one lengthens the other shortens), as observed in other hydrogen-bonded systems. The reported properties, structure-property relations, and molecular understanding provide a foundation for the evolving fundamental understanding and technological advances of these materials.

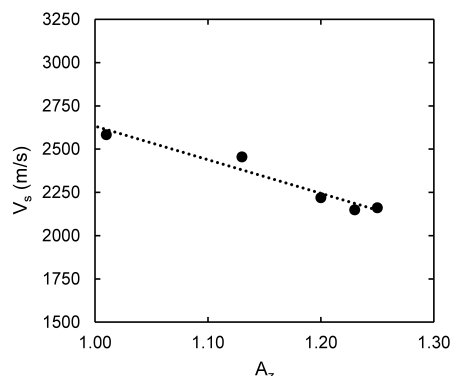


Figure 5. The effect of crystal lattice anisotropy on the shear wave velocity of sII gas hydrates.

Alejandro D. Rey
Department of Chemical Engineering, McGill University
3610 University Street, Montréal, QC
H3A 0C5, Canada
Tel.: +1-514-398-4196
Fax.: +1-514-398-6678
E-mail: alejandro.rey@mcgill.ca

Effect of Guest Size on the Mechanical Properties and Molecular Structure of Gas Hydrates from First-Principles

Thomas M. Vlastic, Phillip D. Servio, Alejandro D. Rey*

Department of Chemical Engineering, McGill University, Montréal, QC, H3A 0C5

*e-mail: alejandro.rey@mcgill.ca

Keywords: Gas hydrates, elastic properties, acoustic properties, hydrogen bonds, ideal strength

Abstract

The elastic and acoustic properties of several sII gas hydrates with hydrocarbon guests (methane, ethane, propane, and isobutane) were investigated and quantified using density functional theory. The shear modulus of ethane-methane hydrates was found to be the highest among all investigated hydrates. Simple (single-guest) hydrates were found to be less resistant to shear stresses than mixed (double-guest) hydrates. In fact, the shear properties (i.e. shear modulus and shear wave velocity) were shown to be closely related to the level of anisotropy in the hydrate crystal lattice, which itself was a function of guest size. A linearly decreasing relationship between the compressional wave velocity and the molecular weight of the guest was also presented. The hydrate crystal structure was analyzed at the atomistic level during triaxial compression and extension. The main findings were that the ultimate tensile strength decreases with guest size, the large cages are more compressible than the small cages, and the bond lengths (H-bonds and O-H bonds) exhibit opposite behaviour (i.e. when one lengthens the other shortens), as observed in other hydrogen-bonded systems. The reported properties, structure-property relations, and molecular understanding provide a foundation for the evolving fundamental understanding and technological advances of these materials.

Introduction

Gas hydrates, or clathrate hydrates, are solid crystalline inclusion compounds that consist of small gas molecules, or volatile liquids, trapped inside a water matrix.¹⁻² The host lattice structure is made up of hydrogen-bonded water molecules that form cage-like structures, in which the guest molecules are enclosed, interacting with the host through van der Waals forces. Natural gas hydrates can be found throughout the world in ocean floor deposits and in permafrost regions that in total result in a greater energy potential than all other available hydrocarbons, while also being a cleaner source of energy.²⁻⁴ Therefore, it is no surprise that gas hydrates are considered a promising future source of energy. Gas hydrates are also of great concern to the oil and gas industry because of their propensity to accumulate and form blockages in pipelines⁵, where temperature and pressure conditions are thermodynamically favorable for hydrate formation. Other important gas hydrate research areas include carbon dioxide sequestration⁶⁻⁷, natural gas transportation and storage⁸, geological hazards⁹, and climate change¹⁰.

Three common forms of gas hydrates exist: structure I (sI), structure II (sII), and structure H (sH). The factors that determine the type of hydrate structure that forms are the temperature and pressure conditions, and the size of the guest molecule in the presence of water.² In nature, the most common hydrates found are methane sI hydrates, however sII gas hydrates, from thermogenic origins, have also been found¹¹⁻¹². Therefore, even though sI gas hydrates have received much more attention, sII gas hydrates are still of great significance, especially since they can also form in man-made structures like oil and gas pipelines, due to the presence of larger hydrocarbons like propane and isobutane. For the successful implementation of any large-scale applications involving gas hydrates, such as the ones previously mentioned, the material properties of gas hydrates are of fundamental importance. The acoustic properties, for example, are necessary for detecting the presence of gas hydrates, whether in natural deposits or in pipelines, and for estimating hydrate composition from seismic data¹³⁻¹⁴. The lack of data on pure gas hydrate properties has led to poorly understood hydrate-bearing sediment mechanical behaviour.¹⁵ Therefore, even in instances where accurate knowledge of hydrate-bearing sediments is the ultimate goal, there is clearly still a need to characterize the material properties of pure gas hydrates, since they are so strongly linked to one another.¹⁵

Few studies have been performed on sII gas hydrate material properties from hydrocarbon formers, such as methane, ethane, propane, and isobutane.¹⁶⁻¹⁷ In fact, as far as the authors could find, only one experimental study¹⁴ exists on the elastic and acoustic properties of sII gas hydrates with hydrocarbon guests. However, only ethane-methane sII hydrates were considered in that study. Although other relevant wave speed data¹⁸⁻²⁰ and elastic constants²¹ have been presented in the literature, the current sII gas hydrate property database remains very limited¹⁵, and in some cases measurements were affected by residual water and gas¹⁹, or by ice²⁰, explaining the large discrepancy in values. Furthermore, only one other first-principles theoretical study²² exists on the mechanical and thermal properties of sII gas hydrates. First-principles modelling has been successfully implemented in many previous gas hydrate studies.²³⁻²⁸ These methods provide the benefit of a thoroughly controlled environment, eliminating impurities and structural defects, where an in-depth investigation into the properties and structure of gas hydrates at the atomistic scale is facilitated. The goal of this paper is to fill the aforementioned gaps in hydrate literature by presenting the elastic and acoustic properties of several sII gas hydrates from hydrocarbon formers (i.e. methane, ethane, propane, and isobutane), using first-principles simulations. The effect of guest size on these properties and on the host crystal lattice structure was also investigated, in compression and in tension, relating molecular level characteristics to macroscopic properties, of relevance to fundamental crystal physics as well as technological applications.

Methodology

Computational method

Computations were performed using the Spanish Initiative for Electronic Simulations with Thousands of Atoms (SIESTA) code which implements density functional theory (DFT). The revised Perdew-Burke-Ernzerhof (revPBE)²⁹ exchange-correlation (XC) functional was used in all simulations. This generalized gradient approximation (GGA) XC functional was chosen based on our previous work^{23,30}, where the performance of several XC functionals were evaluated for gas hydrates. Although GGA functionals do not incorporate long-range van der Waals interactions, in our previous work²³ it was shown for sI methane hydrates that no

improvement in the accuracy of the calculated elastic properties compared to experimental results was observed when taking into account these weaker interactions, such as using the DFT-D2 method³¹. However, the DFT-D2 method does have its downsides³¹⁻³², and the use of newer van der Waals XC functionals may still have significant value in certain cases³³. Double-zeta polarized basis sets and norm-conserving Troullier-Martins pseudopotentials were used. Other noteworthy simulation parameters used were an orbital energy shift of 50 meV, an energy mesh cut-off of 800 Ry, a k-grid cut-off of 10 Å, and a force tolerance of 5 meV/Å.

Structure II gas hydrates are cubic crystals with a unit cell lattice consisting of 136 water molecules, also known as the host, that make up 8 large cages, also referred to as the $5^{12}6^4$ cage (hexadecahedron) and 16 small cages, also referred to as the 5^{12} cage (pentagonal dodecahedron), shown in Figure 1. Trapped inside these cages, gas molecules, also known as the guest, can be found. Due to the high computational cost of DFT and the large number of atoms in the unit cell of sII gas hydrates (i.e. at least 408 atoms), simulations are performed on only a single unit cell lattice with periodic boundary conditions. An initial sII host structure was created using the coordinates provided by Takeuchi et al.³⁴ based on X-ray diffraction results and Bernal-Fowler ice rules. Guest molecules were then placed at the center of the cages, and structure relaxation simulations were performed in order to get the equilibrium structure. Three different types of sII gas hydrates were investigated: empty hydrate, single-guest hydrates (propane and isobutane) also known as simple hydrates, and double-guest hydrates (ethane-methane and propane-methane) also known as mixed hydrates. The sII empty hydrate had no guest, and its equilibrium structure can be seen in Figure 1. The simple hydrates had empty small cages, and 100% large cage occupancy. The mixed hydrates had 100% cage occupancy, where the larger guest occupied the large cages and the smaller guest occupied the small cages. Simulating sII empty gas hydrates is not only a great tool for comparison in order to elucidate the role of the guest-host interactions in hydrate material properties, but empty sII hydrates are no longer purely hypothetical, as they have recently been synthesized experimentally³⁵.

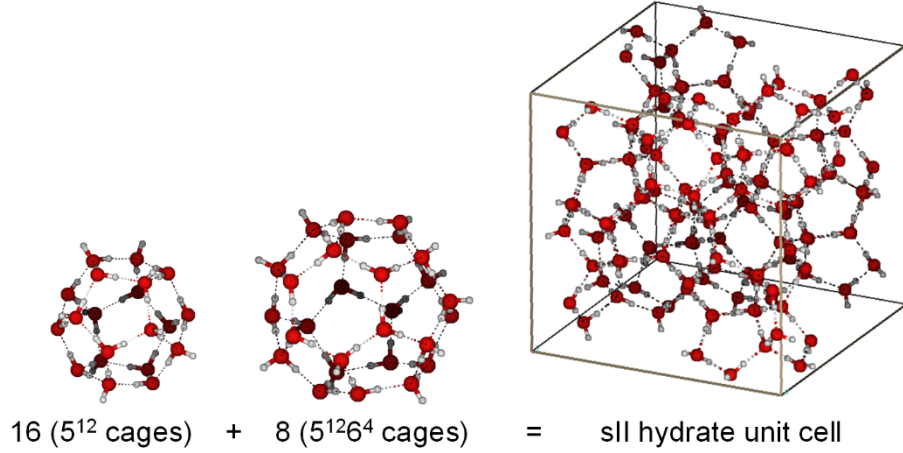


Figure 1. The small 5^{12} cage, the large $5^{12}6^4$ cage, and the equilibrium unit cell lattice of sII empty gas hydrate.

Calculation of elastic constants

Since sII gas hydrates are cubic crystals, they have three independent second-order elastic constants: c_{11} , c_{12} , and c_{44} . The elastic constants were calculated using the energy approach as discussed by Stadler et al.³⁶ and Jamal et al.³⁷. In this method, three independent strains $\varepsilon(\delta)$ must be applied to the unit cell, since there are three independent elastic constants. Each given strain will cause a change in total system energy. This change in energy from the unstrained system can be expressed in a Taylor series as a function of the elastic strain, presented in equation 1.

$$\Delta E = \frac{V_0}{2} \sum_{i=1}^6 \sum_{j=1}^6 c_{ij} \varepsilon_i \varepsilon_j + O(\varepsilon_i^3) \quad (1)$$

where ΔE is the change in energy due to the strain vector ‘ ε ’, which in Voigt notation is $\varepsilon = (\varepsilon_1, \varepsilon_2, \varepsilon_3, \varepsilon_4, \varepsilon_5, \varepsilon_6)$, c_{ij} are the elastic constants, and V_0 is the equilibrium volume. The three sets of strains used in this analysis were a volume-conserving tetragonal strain $\varepsilon_1 = (\delta, -\delta, \frac{\delta^2}{1-\delta^2}, 0, 0, 0)$, a [110] strain $\varepsilon_2 = (\delta, \delta, 0, 0, 0, 0)$, and a [111] shear strain $\varepsilon_3 = (0, 0, 0, \delta, \delta, \delta)$. These three strains, when inserted into Equation 1, result in three different energy-strain equations, Equation 2, 3, and 4, respectively:

$$\Delta E = V_0(c_{11} - c_{12})\delta^2 + O(\delta^4) \quad (2)$$

$$\Delta E = V_0(c_{11} + c_{12})\delta^2 + O(\delta^2) \quad (3)$$

$$\Delta E = \frac{3V_0}{2}c_{44}\delta^2 + O(\delta^2) \quad (4)$$

Finally, for each independent strain $\epsilon(\delta)$, the change in system energy was plotted versus the strain δ , and a polynomial in δ was fit to the data. The second order coefficient of each fitted polynomial is set equal to the coefficient of the corresponding energy-strain equation, and the elastic constants are then solved. It should be noted that these elastic constants describe the elastic behaviour of a single gas hydrate crystal. However, the Voigt-Reuss-Hill approximation, describing the elastic properties of polycrystalline solids from monocrystalline elastic constants, were used to calculate the bulk modulus and the shear modulus of polycrystalline sII gas hydrates.³⁸ Furthermore, elastic relations for isotropic solids were then used to calculate other elastic and acoustic properties such as Young's modulus, Poisson's ratio, compressional and shear wave velocities. The equations used to calculate these material properties are presented in the Supporting Information.

Results and Discussion

Elastic constants and properties

The second-order elastic constants resulting from the energy-strain analysis described in the previous section are presented in Table 1, along with relevant literature values. An example of the data for sII empty hydrate used to calculate these elastic constants can be found in the Supporting Information, in graphical format (Figure S1). A set of three similar graphs was obtained for each sII gas hydrate.

Table 1. Second-order elastic constants of sII gas hydrates monocystals, with relevant available literature data.

	Empty	Propane	Isobutane	Ethane-methane	Propane-methane
c_{11} (GPa)	19.3	16.2	14.9	16.9	15.7, 15.3 ^a
c_{12} (GPa)	8.0	8.6	7.2	6.1	6.9, 7.0 ^a
c_{44} (GPa)	5.7	4.8	4.7	6.1	5.3, 4.6 ^a
Zener anisotropy factor A_z	1.01	1.25	1.23	1.13	1.20
Every anisotropy factor A_e	-0.01	-0.16	-0.18	-0.13	-0.17

^a Huo et al. (2011), Ref. ²²

The elastic constants in Table 1 are in good agreement with data available in the literature, namely for propane-methane hydrates both theoretical²² and experimental²¹. There is a small difference in the c_{44} elastic constant, which represents shear in the 100 plane. The discrepancies in elastic constants could be attributed to the fact that we used norm-conserving pseudopotentials while Huo et al.²² used ultrasoft pseudopotentials. From Table 1, it can be seen that the c_{11} and c_{44} elastic constants generally decrease with increasing guest size. However, unlike for the c_{11} elastic constant, the addition of a guest in the small cage increases the c_{44} constant. The ethane-methane sII hydrate does not follow this trend, and appears to have unique shear properties (i.e. c_{44} is the highest, even more so than for the empty hydrate). In fact, when comparing the sII elastic constants to sI methane hydrate elastic constants calculated from a similar theoretical method ($c_{11}=18.1$, $c_{12}=5.7$, and $c_{44}=6.2$)²³, ethane-methane sII hydrates stand out as being the most similar. This is somewhat unsurprising as the guest molecules are the most similar.

For a perfectly isotropic cubic crystal, the Zener anisotropy factor (A_z) is equal to one and the Every anisotropy factor (A_e) is equal to zero.³⁸ These two quantities cannot be made a function of one another, and can therefore both serve as measures of anisotropy.³⁸ Empty sII hydrates are almost perfectly isotropic as $A_z \approx 1$ and $A_e \approx 0$. The sII hydrates begin to deviate from a perfect isotropic cubic structure as guest size increases. In other words, the sII gas hydrates become more anisotropic, as indicated by an increase in the Zener anisotropy factor A_z and a decrease in the Every anisotropy factor A_e . The relationship between A_e and large cage guest diameter can be seen in Figure 2. However, the five sII gas hydrates under investigation are all

still nearly isotropic, since $1.00 < A_z < 1.25$ and $-0.18 < A_e < 0$. The same observation regarding the nearly isotropic nature of gas hydrates was also made by Shimizu et al.³⁹ and Sasaki et al.²¹

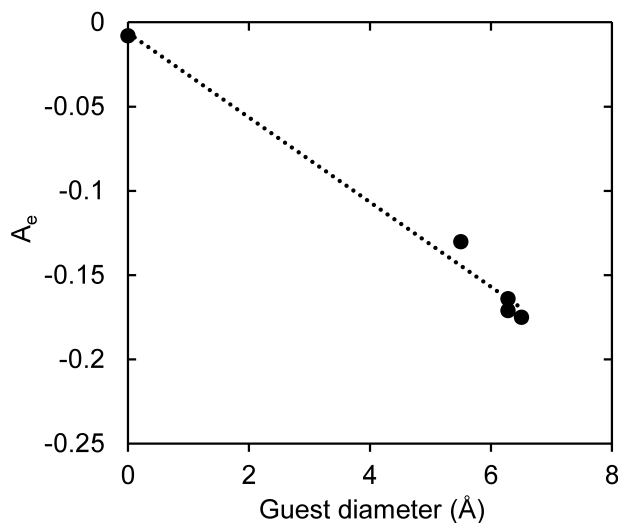


Figure 2. The Every anisotropy factor (A_e) as a function of large cage guest diameter for sII gas hydrates (Note: guest diameters taken from Sloan and Koh 2007²).

The importance of Figure 2 is in the trend that can be observed, which shows that crystal lattice anisotropy increases as guest size increases, and not necessarily from the equation of the line. It should be noted that the difference between guest size in the large cage and small cage will also have an impact on anisotropy. For example, methane sI hydrates were found to have $A_e \approx 0$ with 100% cage occupancy²³, even though a methane molecule is 4.36 Å in diameter². Therefore, it could be expected that sII gas hydrates with 100% cage occupancy of a guest with a similar or smaller size than methane (e.g. hydrogen, oxygen, nitrogen) would have a similar measure of anisotropy as the sII empty hydrate, not necessarily indicative of the size of the molecule. One may need to take into account not only the size of the guest and the size difference between the guests in each type of cage, but also the guest-to-cage ratio.

A summary of the polycrystalline mechanical properties for the sII gas hydrates under investigation can be found in Table 2, along with relevant values from the literature. As mentioned above, very little data currently exists on the elastic properties of sII gas hydrates,

however in the instances where data is available^{14, 22}, the results are in good agreement with our work.

Table 2. Polycrystalline mechanical properties of sII gas hydrates, with relevant available literature values.

	Empty	Propane	Isobutane	Ethane-methane	Propane-methane
Lattice constant a_0 (Å)	16.85	17.09	17.28	17.21	17.33, 17.72 ^a
Bulk modulus B_0 (GPa)	11.75	11.14	9.76	9.70, 8.51 ^b	9.84, 9.76 ^a
Shear modulus G (GPa)	5.68	4.36	4.34	5.79, 3.68 ^b	4.89, 4.43 ^a
Young's modulus E (GPa)	14.67	11.57	11.33	14.48, 13.41 ^b	12.58, 11.55 ^a
Compressional wave velocity V_p (km/s)	4.767	4.263, 3.698 ^c	4.070	4.258, 3.822 ^b	4.093, 4.141 ^a
Shear wave velocity V_s (km/s)	2.584	2.162	2.150	2.455, 2.001 ^b	2.237, 2.203 ^a
Poisson ratio ν	0.292	0.327	0.306	0.251, 0.311 ^b	0.287, 0.303 ^a
Density ρ (Kg/m ³)	850.3	932.9	938.4	960.8, 917 ^b	976.1, 910.0 ^a

^a Huo et al. 2011, Ref. ²²

^b Helgerud et al. 2009, Ref. ¹⁴

^c Kieft et al. 1985, Ref. ¹⁸

The mechanical properties of propane-methane hydrate presented in Table 2 correspond very well to the theoretical results obtained by Huo et al.²² for the same sII hydrate structure. The small difference in the shear and Young's moduli for the polycrystalline propane-methane hydrate can be attributed to the difference in the elastic constant c_{44} , as previously discussed. When compared to experimental results, in the case of ethane-methane sII hydrates¹⁴, the polycrystalline material properties are similar, but larger differences can be observed. Likewise, the compressional wave speed of 4.263km/s found for propane hydrates is larger than the value of 3.698 km/s found by Kieft et al.¹⁸. This can be attributed to differences in temperature and pressure conditions. It should be noted that first-principles calculations are performed at a temperature of 0 K and a pressure of 0 GPa, analogous to atmospheric pressure, while the experimental results for ethane-methane sII hydrate were obtained at a temperature of 273 K and

a pressure of 30.5 MPa. The elastic properties of sII gas hydrates (i.e. elastic moduli, and wave velocities) have been shown to decrease with increasing temperature.^{14, 40} Therefore, we would expect systematically higher values at a temperature of 0 K. An exception to this rule was recently reported by Jia et al.⁴¹ for carbon dioxide sI hydrates where the shear modulus and Young's modulus were found to decrease with increasing temperature. However, this is anomalous behaviour for crystalline materials, which in general lose their rigidity as temperature increases, and exhibit softening of the crystal lattice until it transforms into a liquid.⁴¹ The sII gas hydrates investigated in this work therefore appear to exhibit normal crystalline behaviour. Furthermore, Helgerud et al.¹⁴ reported a 94% cage occupancy for their experimentally synthesized ethane-methane hydrates while the nature of our simulations requires a cage occupancy of 100%, which can also cause differences in mechanical properties^{2, 42}. Another point worth mentioning is that the ethane-methane mixed hydrate simulated in this work was assumed to have 100% large cage occupancy of ethane. However, in reality methane can also occupy the large cages. This could change the calculated mechanical properties, such as crystal anisotropy, shear modulus, and shear wave velocity, among possible others (i.e. as a result of methane occupying some of the large cages as well as all the small cages, crystal anisotropy could decrease, and shear wave velocity could increase). Therefore, the assumption of 100% occupancy of large cages by ethane can also lead to slight differences in material properties between theoretically and experimentally investigated ethane-methane hydrates. Molecular dynamics could be a great tool to study this effect as it can handle much larger systems than DFT, and would therefore be more feasible to study mixed hydrates with varying large cage occupancy. In DFT, the system is too small to introduce enough randomness into the structure.

Compared to our previous work on sII gas hydrates³⁰, where we used the equation of state approach to calculate the equilibrium volume and the bulk modulus, the results are extremely similar, validating the consistency between the two different methods. This similarity between methods was also found for sI hydrates.²³ However, for the propane guest molecule, the bulk modulus is slightly different depending on the approach. We hypothesize this to be because of the larger internal stresses found in the propane hydrate and the propane-methane hydrate, where the equilibrium lattice angles deviate the most from the perfect 90° cubic angles, out of the five sII hydrates considered in this work. Although the butane molecule is larger, it has a more

spherical shape than the propane molecule, and may affect the hydrate cubic lattice in a more isotropic manner. As was shown earlier in this section for the elastic constants, the polycrystalline properties of sI methane hydrates²³ most resemble the properties of ethane-methane sII hydrates, which again is unsurprising due to the similarities in their compositions. Furthermore, the experimental polycrystalline elastic properties found by Helgerud et al.¹⁴ are also extremely similar for methane sI hydrates and ethane-methane sII hydrates, further validating the trend we have observed using first-principles theoretical modelling.

While isobutane hydrates are more compressible than propane hydrates (i.e. lower bulk modulus, as seen in Table 2), they appear to have the same shear properties. In fact, simple sII gas hydrates are significantly easier to shear as indicated by their lower shear modulus. On the other hand, mixed sII hydrates with guests of similar size have a higher shear modulus (as long as they are relatively small), as is the case for ethane-methane hydrate. This interesting result arises due to the difference in size between the guests in each cage, which could mean that the shear modulus is also tied to the level of anisotropy in the crystal lattice. Therefore, mixed hydrates should be able to resist shear stresses more effectively than simple hydrates, which is analogous to analyzing cage occupancy. This is true for sI methane hydrates, with 100% occupancy, which were found to have a shear modulus of 6.23 GPa²³, using *ab initio* modeling, greater than any of the values for the hydrates investigated in this work. Sasaki et al.²¹ also came to the conclusion that methane sI hydrates have a greater shear strength than propane-methane hydrates. The size and shape of the guest molecule have to be considered as well. For example, carbon dioxide is a larger molecule than methane, resulting in a larger guest-to-cage ratio, and has a linear shape. As a result, carbon dioxide sI hydrates have a significantly lower shear modulus (3.98 GPa), and are less isotropic, than sI methane hydrates²³, even though both hydrates had 100% occupancy.

It is clear from the results in Table 2 that the size of the guest molecules and the type of hydrate (simple versus mixed) have an effect on the material properties of sII gas hydrates. An in depth analysis of this effect on the bulk modulus was performed in our previous work³⁰, where hydrogen-bond density and bulk modulus were found to be linearly correlated. This size effect

also becomes noticeable when analyzing the compressional wave velocities, which is the focus of the next section.

Wave Velocities

Kieft et al.¹⁸ found that the compressional wave velocity of gas hydrates increases as the molecular weight of the guest decreases. Helgerud et al.¹⁴ later developed this observation into a relationship, shown in Equation 5, between the compressional wave velocity in gas hydrates and the square root of the molecular weight of the guest molecule at 0°C:

$$V_p = 4019 - 46.59\sqrt{m_{\text{guest}}} \quad (5)$$

where V_p is in $\text{m}\cdot\text{s}^{-1}$ and m_{guest} is in $\text{g}\cdot\text{mol}^{-1}$. Similarly, from Table 2 this relationship is also evident, illustrated in Figure 3, where compressional wave velocity is shown to be a function of the average molecular weight of the guest in each cage in the sII gas hydrates investigated in this work.

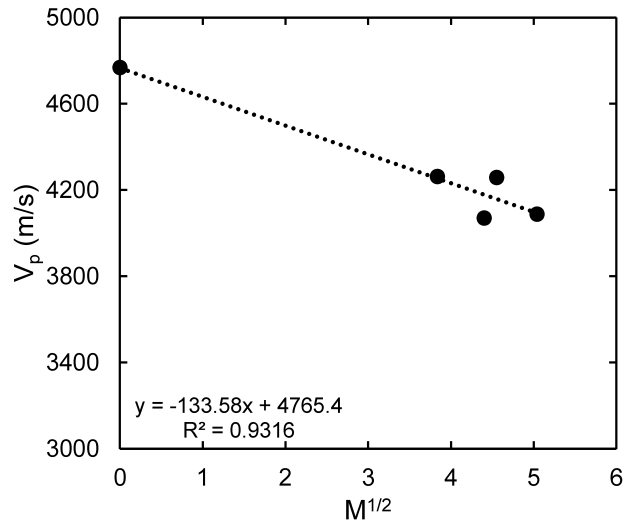


Figure 3. Relationship between the compressional wave velocity in sII gas hydrates and the average molecular weight (in $\text{g}\cdot\text{mol}^{-1}$) of the guest molecule in each cage.

While the slope and intercept differ from the equation presented by Helgerud et al.¹⁴ due to temperature effects, as can be seen in Equation 6, the general form of the relationship still holds:

$$V_p = 4765.4 - 133.58\sqrt{m_{\text{guest}}} \quad (6)$$

where V_p is in $\text{m}\cdot\text{s}^{-1}$ and m_{guest} is in $\text{g}\cdot\text{mol}^{-1}$. It should be noted that the relationship presented by Helgerud et al.¹⁴ from the results of longitudinal acoustic velocities for sII gas hydrates by Kieft et al.¹⁸ was developed based on simple hydrates only: propane, THF, Freon-11, and sulfur hexafluoride. In this work, we present the acoustic velocities of both simple and mixed hydrates. When attempting the same analysis with shear wave velocities, the relationship is not as obvious or compelling, as can be seen in Figure 4. As previously mentioned, shear properties are highly dependent on cage occupancy (i.e. simple hydrate, where 8/24 cages are occupied, versus mixed hydrate, where all cages are occupied).

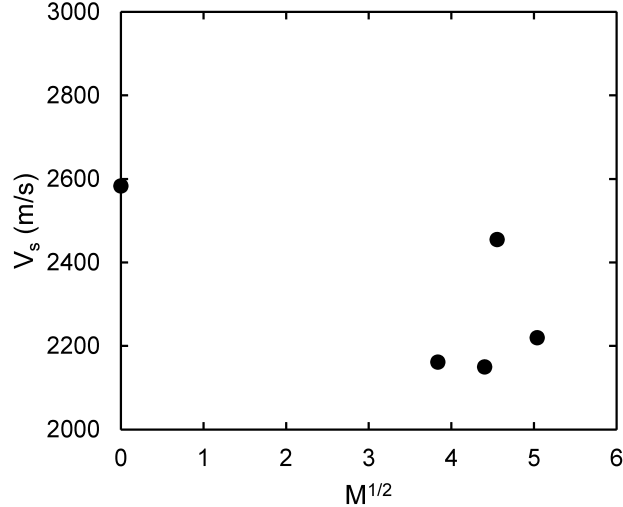


Figure 4. Relationship between the shear wave velocity in sII gas hydrates and the average molecular weight (in $\text{g}\cdot\text{mol}^{-1}$) of the guest molecule in each cage.

Furthermore, in the previous section, we argued that the level of anisotropy in the hydrate crystal has a significant effect on its shear properties (i.e. shear modulus). Therefore, it follows

that the shear wave velocity could also depend on the anisotropy of the crystal lattice. This dependence is confirmed in Figure 5.

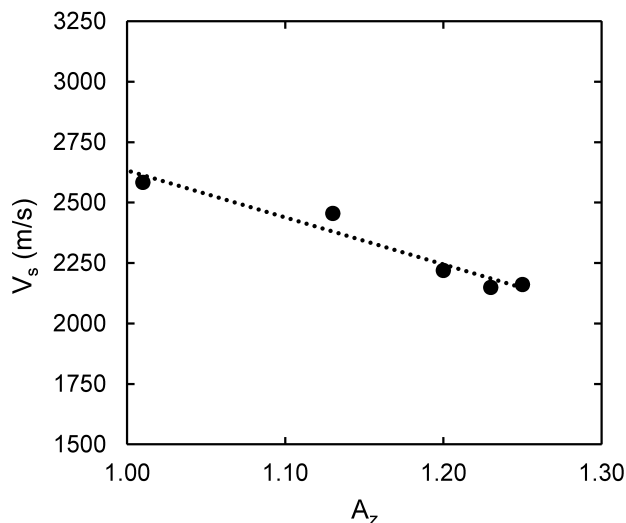


Figure 5. The effect of crystal lattice anisotropy on the shear wave velocity of sII gas hydrates.

Hydrate Atomic Structure

Now that we have analyzed the effect of the guest molecules trapped in the gas hydrate lattice on the monocrystalline and polycrystalline properties, we also wanted to analyze their effect on the atomic structure under tensile and compressional stresses in terms of bond lengths and bond angles. This can give us more insight into the structural strengths and weaknesses of each individual sII gas hydrate, as well as in comparison to sI gas hydrates and ice.

We found that the maximum tensile stress before hydrogen-bond breakage, signifying the onset of the collapse of the crystal lattice, is different depending on the guest in sII hydrates. An example of this maximum stress can be seen in Figure 6a-c for propane hydrates where the bond lengths eventually reach a vertical asymptote at a certain stress. These three figures illustrate the effect of hydrostatic compression and extension on the average bond lengths in propane hydrates, with error bars representing the total spread of values in the unit cell. The total spread of values for the hydrogen bonds and the O-O distances increases significantly as the hydrate's maximum tensile strength is approached, because some of the weaker hydrogen bonds become subjected to

stresses which are near to or beyond their maximum strength, and therefore lengthen significantly upon even the smallest increase in tensile stress.

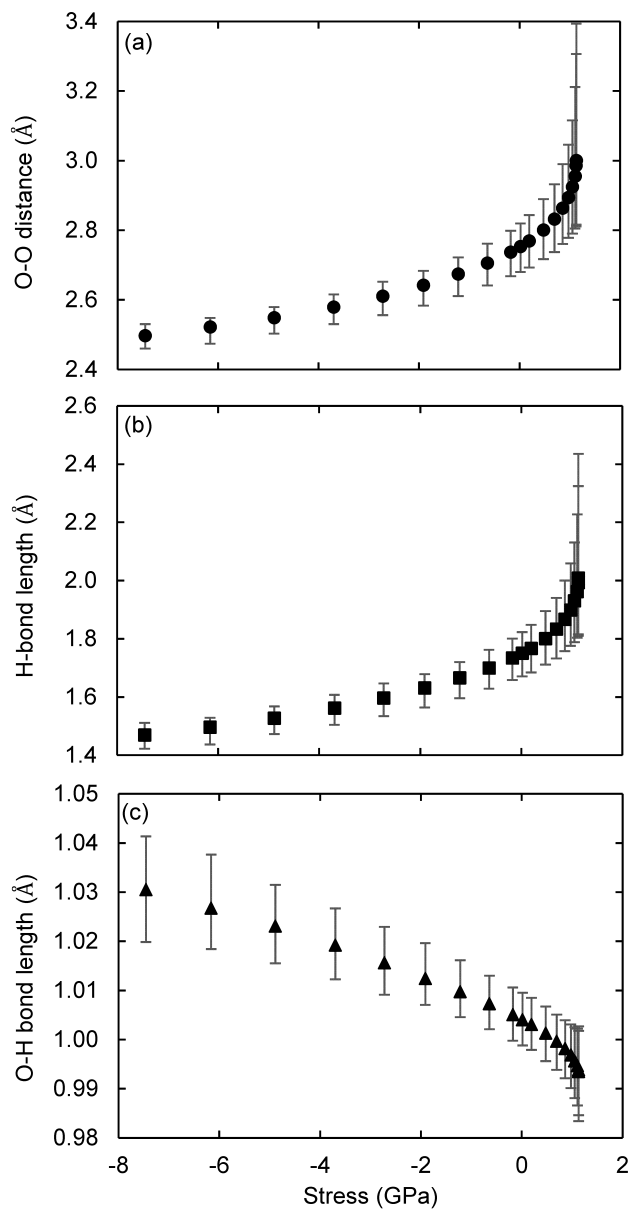


Figure 6. Average bond lengths in propane sII hydrate under triaxial stress, with error bars representing the total spread of values: a) O-O distance, b) hydrogen bond length, and c) covalent O-H bond length.

The bond lengths of all other sII gas hydrates considered in this work are presented in Figure S2 in the Supporting Information. The maximum tensile stress, or ultimate tensile

strength, for the sII gas hydrates under investigation is shown in Table 3. From this analysis, it can be seen that empty sII hydrates are capable of withstanding the greatest tensile stresses, identical to the conclusion made for sI hydrates²⁴. Upon compression, however, the repulsive effect of the guest molecules allows the lattice structure to withstand much higher compressional stresses, which is not the case in empty sII hydrates. A high compressional strength combined with a weak tensile strength reveals the brittle nature of gas hydrates.²⁴

Table 3. The molecular structure of sII gas hydrates at their ultimate tensile strength.

sII hydrate guest	Tensile strength (GPa)	Lattice constant (Å)	Average H-bond length (Å)	Average O-H bond length (Å)
Ethane-methane	1.10	19.0	2.063	0.991
Propane-methane	1.02	18.9	2.045	0.992
Empty	1.26	18.8	2.026	0.993
Propane	1.13	18.7	2.009	0.994
Isobutane	0.98	18.5	1.976	0.995

The empty sII hydrate unit cell lattice, at its ultimate tensile strength, can be visualized in Figure 7, where a further increase in triaxial tensile stress starts to break the hydrogen bonds of the large cages. Therefore, the large cages appear to be less resistant to tensile stresses than the small cages. An identical observation was made for the four other sII hydrates under investigation.

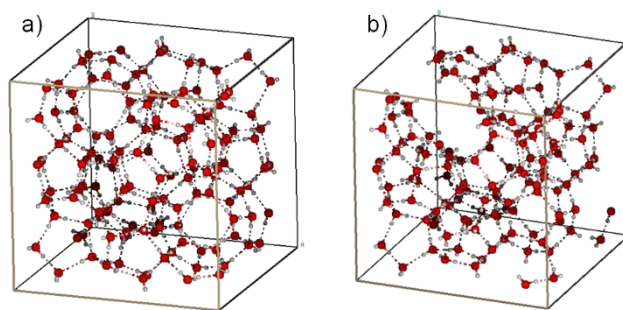


Figure 7. Empty sII hydrate unit cell under triaxial tension at its ultimate tensile strength: a) before lattice destabilization and b) after lattice destabilization due to hydrogen bond breakage.

The difference in ideal tensile strengths seen in Table 3 would suggest that the hydrogen bonds in a hydrate with a smaller guest (e.g. propane) are stronger than the hydrogen bonds in a hydrate with a larger guest (e.g. isobutane), because it takes more force to pull them apart. This is also validated by the differences in their bulk moduli (11.14 GPa for propane hydrate versus 9.76 GPa for isobutane hydrate) and in their Young's moduli (11.57 GPa for propane hydrate versus 11.33 GPa for isobutane hydrate). Again, this could be due to the repulsive effect of the guest molecule on the surrounding cage of hydrogen-bonded water molecules. Therefore, in tension, the repulsive effect of the guest causes a weakening of the lattice structure, while in compression, it causes a strengthening of the lattice structure. However, the lattice constants at which the sII hydrates break upon extension and cause lattice destabilization follow a slightly different trend than the ultimate tensile strengths, and are shown in Table 3. This trend is also reflected in the average hydrogen-bond length at the ultimate tensile strength, seen in Table 3. It can be seen that having a guest in the small cage (e.g. methane) can increase the stability of the hydrate crystal and allow for a greater average H-bond length and lattice volume, at the ultimate tensile strength. Therefore, both tensile strength and maximum volume depend on the properties of the H-bond (i.e. how much it can stretch and elongate without breaking), however the maximum volume also depends on the stabilizing effect of the guest molecules, while the ultimate tensile strength is purely a function of guest size. The stabilizing effect of the guest molecule will depend on guest size, because of the interplay between repulsive and attractive van der Waals forces.

Having a larger guest in the large cage leads to a greater destabilization of the hydrate structure in tension and causes a shorter H-bond length at the ultimate tensile strength. Since there are 16 small cages and only 8 large cages in the unit lattice, the guests in the small cages have a greater influence, as can be seen by the fact that propane-methane and ethane-methane hydrates are stable at a larger volume than the empty hydrate. Further evidence of this can be seen in Figure 8a, where the size of the small cages, as the sII gas hydrates reach their ultimate tensile strength, follows the same trend as in Table 3, while the size of the large cages follows the opposite trend, shown in Figure 8b. This means that ethane-methane hydrates have the smallest difference in cage size (large cage versus small cage), while isobutane hydrates have the

largest difference in cage size, helping to further explain the differences in their shear properties presented earlier.

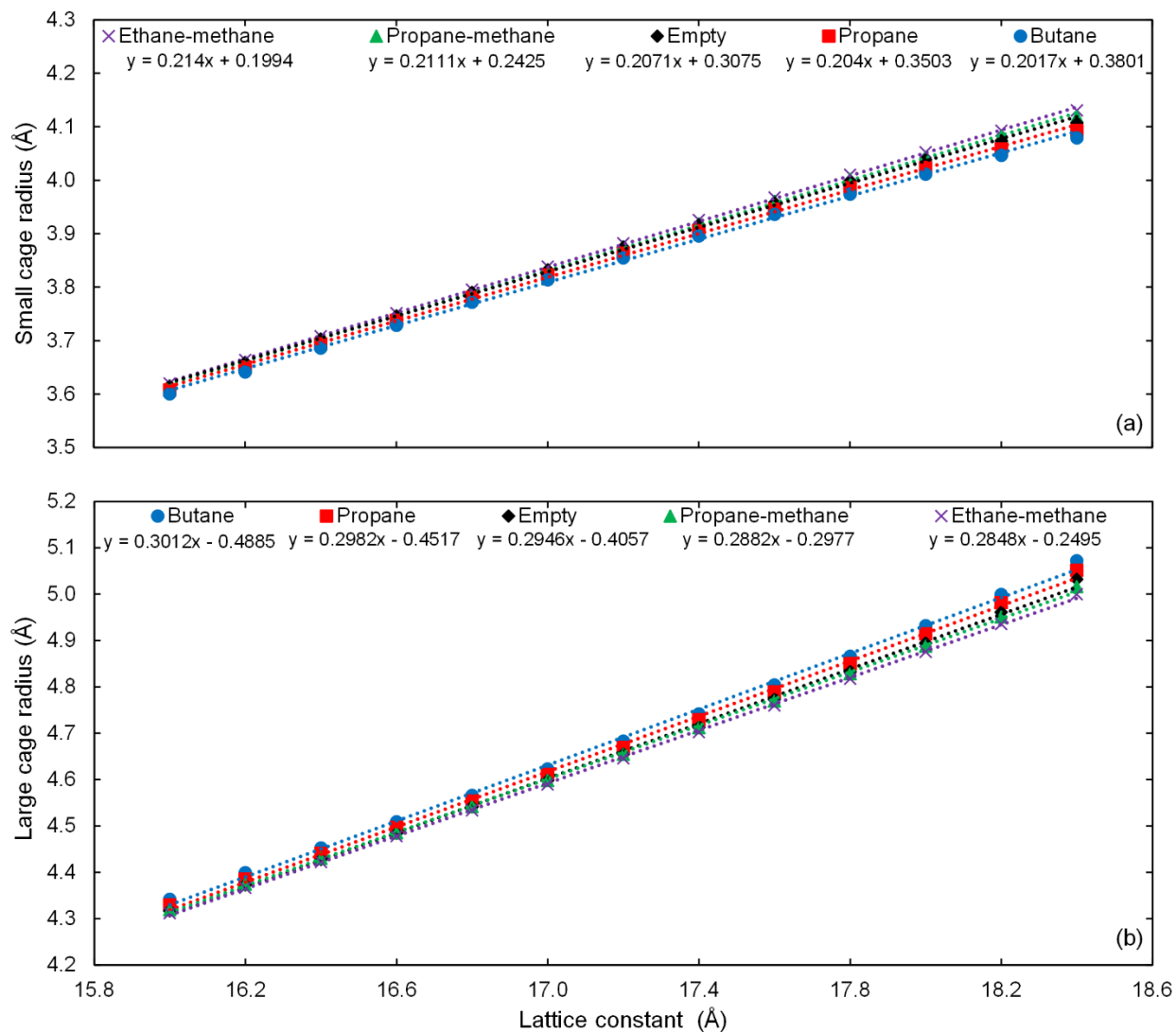


Figure 8. The relationship between cage radius and lattice size of sII gas hydrates: a) small cages and b) large cages.

Furthermore, Figure 8 shows a linear relationship between the radii of the cages and the lattice size. This observation validates the assumption that the cage radii are a linear function of the lattice constant made by Ballard et al.⁴³ in an attempt to improve upon the van der Waals-Platteeuw thermodynamic model for gas hydrate formation prediction. However, the slope of the

line depends on the size of the guest, and the type of cage. For one, the large cages in any given sII hydrate are more sensitive to changes in pressure than the small cages, as seen by the larger slopes in Figure 8b, which means they are more compressible. Izquierdo-Ruiz et al.²⁸ and Klapproth et al.⁴⁴ came to the same conclusion regarding the compressibility of the two types of cages in carbon dioxide and methane sI hydrates, respectively: the large cages (6^25^{12}) are more compressible than the smaller ones (5^{12}), and with an increase in pressure comes an increase in the ratio of small cage volume to large cage volume. When one type of cage is most sensitive to the presence of a guest molecule, it follows that the other type is least sensitive, and vice versa, as suggested by the opposite trends in slopes for the five sII gas hydrates in Figures 8a-b. The equilibrium cage radii are in good agreement with available data in the literature. For example, Kumar et al.⁴⁵ found an empty 5^{12} cage to be 3.85 Å in radius, and Sloan et al.² presented a value of 3.91 Å for the sII small cage and 4.73 Å for the large cage, while our results are 3.79 – 3.92 Å for the small cage and 4.54 – 4.71 Å for the large cage depending on the type of guest.

Going back to Figures 6a-b, it can be seen that as the system is isotropically compressed the O-O distances and the hydrogen bond lengths decrease, respectively. However, in Figure 6c, it can be seen that the O-H covalent bond lengths increase with increasing pressure. This is somewhat different to what was observed in our previous work²⁴ for uniaxial compression of sI methane hydrates, where the O-O distances and hydrogen bond lengths initially decrease upon compression, however with further compression the bond lengths reach a minimum and begin to increase. Likewise, the covalent bond lengths increase upon compression eventually reaching a maximum and then begin to decrease upon further uniaxial compression of sI methane hydrates. On the other hand, no significant difference was observable in the structural changes whether the gas hydrate lattice was subjected to uniaxial or triaxial tensile stress. The overall recurring theme is that the H-bond and the O-H covalent bond lengths change in opposite directions (see Figure S2 in the Supporting Information). In fact, it is well known that in hydrogen bonding systems, as the hydrogen bond length decreases (and as the total O-O distance decreases) the covalent bond length increases.⁴⁶⁻⁴⁹ As the system is being compressed, the O-O distance inevitably decreases, as the hydrogen-bonded water molecules are forced closer together. Since the hydrogen bond is weaker, and therefore more compressible than the covalent bond, this causes the hydrogen bond to decrease in length as pressure increases. As the hydrogen bond decreases in length, it becomes

stronger, and consequently has a stronger pull on the covalently bound hydrogen atom. This then causes the covalent bond to weaken and therefore lengthen.

In Figure 9, it can be seen that as compressive stress increases, the difference in length between the H-bond and the O-H bond decreases. Theoretically, this could continue as pressure is increased until both bonds reach equal length, provided that the hydrate lattice remains stable. Also known as length symmetrisation, or hydrogen bond symmetrisation, this phenomenon was hypothesized in 1972⁵⁰ and experimentally confirmed in 1998⁵¹ for ice under 60 GPa of pressure at 100 K.

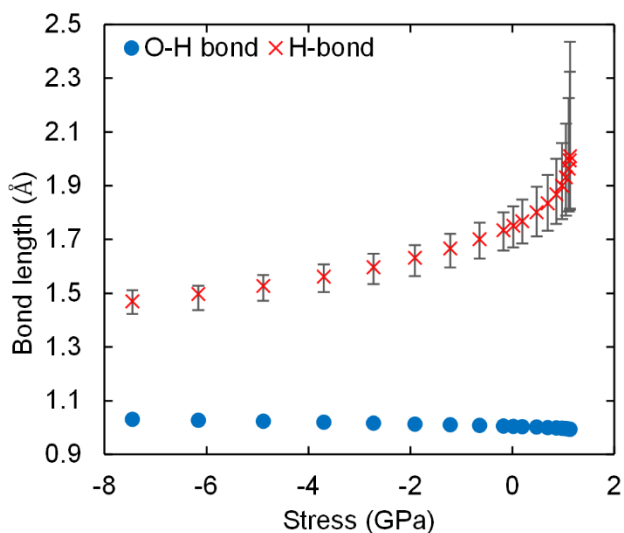


Figure 9. Length symmetrisation in propane sII hydrate under triaxial stress (i.e. both bonds tend towards equal length under increasing compressive stress).

A more compelling depiction of length symmetrisation can be seen in Figure 10, where the dependence of each individual average bond length is shown as a function of the overall O-O average distance for isobutane hydrate. The trend observed in Figure 10 is extremely similar to that observed by Goryainov et al.⁴⁹ showing the theoretical dependences of the O-H and H-bond lengths on the total O-O distance as well as experimental data of crystals⁵²⁻⁵³. The figure presented by Goryainov et al.⁴⁹ also shows the two bond lengths meeting at an O-O distance of 2.4 Å, where each bond would be 1.2 Å in length. Although Figure 10 seems likely to corroborate this observation, the isobutane hydrate lattice was no longer stable at an O-O

distance below 2.5 Å. The lattice became too compressed and had to rearrange by breaking bonds and reordering. The same behaviour was observed for all other sII gas hydrates under investigation (see Figure S3 in the Supporting Information). Therefore, although length symmetrisation could theoretically also occur for sII gas hydrates, there would inevitably be a change in lattice configuration, and the lattice structure would no longer be typical of structure II gas hydrates.

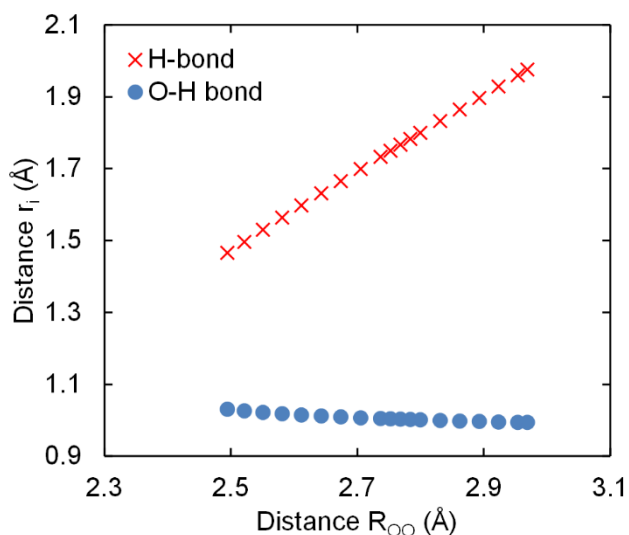


Figure 10. The dependence of the average hydrogen bond and covalent bond lengths on the average O-O distance in sII isobutane hydrate.

Figure 11 illustrates the average O-O-O angles in sII gas hydrates, upon isotropic compression and extension, with error bars representing the total spread of O-O-O angles in the unit cell. The sII hydrate structure does not vary significantly from the ideal tetrahedral arrangement of 109.5° throughout the entire range of compressional and tensile stresses, as seen in sI methane hydrates, but unlike ice Ih²⁴. This means that the lattice of ice Ih is better suited to adapting to applied stresses, by slightly reorganizing its internal structure without mechanical failure. However, both sI²⁴ and sII structures remain rigid and virtually unchanged, suggesting they will likely be unable to withstand the same stresses without sudden structural failure. We found that the propane hydrate deviates by 0.004% and 0.12% from its equilibrium average bond angles under tension and compression, respectively, while ice Ih deviates by 0.25% under tension, and 1.38% under compression²⁴. That change in bond angles is over 60 times greater

under tension, and over 10 times greater under compression for ice Ih than for propane hydrates, demonstrating the rigidity of the hydrate structure.

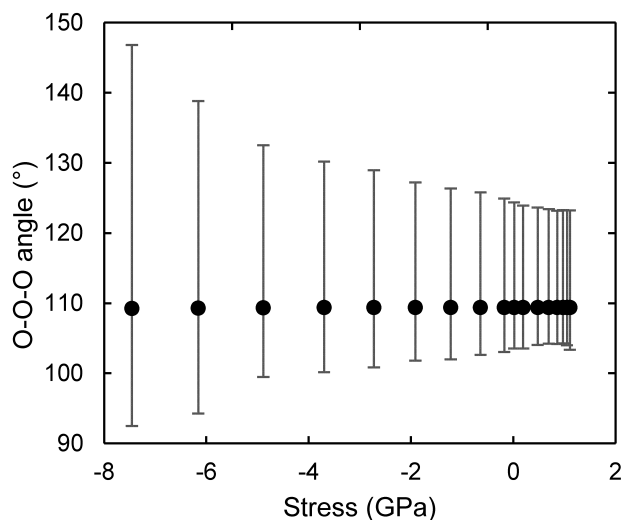


Figure 11. Average O-O-O angles in sII propane hydrate under triaxial stress, with error bars representing the total spread of O-O-O angles in the unit cell.

Although the average O-O-O angles in sII gas hydrates do not vary significantly from 109.5° , it should be noted that two different categories of O-O-O angles exist: pentagonal face angles and hexagonal face angles. This explains why gas hydrates have a greater variability in bond angles than ice Ih²⁴, and also why the total spread of values shown by the error bars in Figure 11 is so large. Upon compression, the spread becomes even larger, because the cages begin to warp causing some O-O-O angles near the maximum value to increase and others near the minimum value to decrease. Figure 12 illustrates the O-O-O angles in sII propane hydrates in their respective category, with error bars representing the total spread of O-O-O angles in the unit cell. A perfect pentagonal angle is 108° , and a perfect hexagonal angle is 120° . As can be seen in Figure 12, the average O-O-O angles in sII propane hydrates do not vary from their respective ideal angles upon isotropic compression and extension. However, the variability within each category increases not only with increasing compressive stress, but also with increasing guest size (see Figure S4 in the Supporting Information).

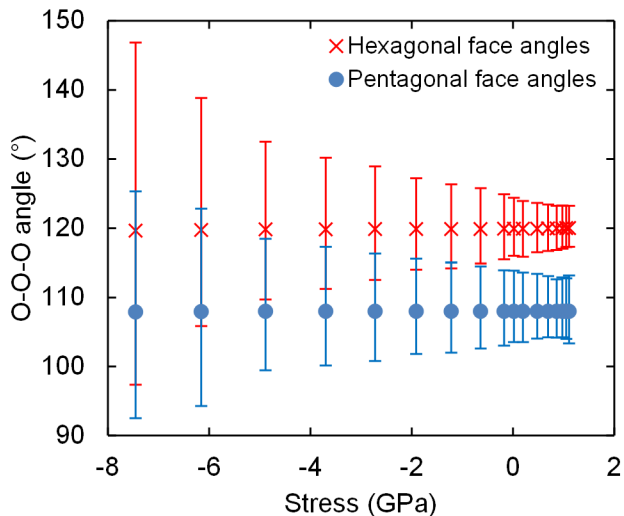


Figure 12. O-O-O bond angles in sII propane hydrate under triaxial stress, with error bars representing the total spread of O-O-O angles in the unit cell.

A summary of the bond lengths and angles under zero stress for all sII gas hydrates under investigation can be found in Table 4, in order to analyze the effect of guest size. With an increase in guest size comes an increase in the O-O distance as well as in the H-bond length, but a decrease in the O-H covalent bond length. The empty sII O-O distance of 2.716 Å corresponds well to the average value of 2.72 Å found by Kumar et al.⁴⁵ for the empty dodecahedral water cage. Our average equilibrium bond lengths and angles for sII hydrates are also in agreement with other theoretical and experimental results for sI hydrates and ice Ih^{24, 28, 54}. While neither the pentagonal face angles nor the hexagonal face angles in sII gas hydrates deviate significantly from the ideal arrangement, regardless of guest size, there is slightly more change in the angles of the hexagonal faces. Therefore, the hexagonal faces, and by extension the large cages, appear to be more compliant, and it is likely that they would be the first to rearrange upon added stress. This observation is also corroborated by the fact that the large cage radii are more sensitive to changes in pressure and that the hydrogen bonds of the large cages are the first to break upon added triaxial tensile stress beyond the hydrates' ultimate tensile strength, as mentioned previously. It is no coincidence that the small cage (i.e. the pentagonal dodecahedron) is the only cage found in all three of the most common structures of gas hydrates (i.e. sI, sII, and sH).

Table 4. Average equilibrium bond lengths (Å) and angles (°) for sII gas hydrates

	Empty	Propane	Isobutane	Ethane-methane	Propane-methane
O-H covalent bond	1.007	1.004	1.002	1.003	1.001
Hydrogen bond	1.710	1.749	1.780	1.772	1.793
O-O distance	2.716	2.752	2.781	2.773	2.793
O-O-O angles	109.39	109.39	109.26	109.39	109.39
Pentagonal face angles	107.99	107.99	107.98	107.99	107.99
Hexagonal face angles	119.84	119.89	119.92	119.85	119.87

Conclusions

The mechanical properties presented in this work are a significant contribution to the extremely limited database of sII gas hydrate material properties. These results provide important insight into the differences between the elastic properties of specific gas hydrates, for example how resistant to shear stresses each of them is, and by extension how hydrate-bearing sediments may behave depending on their composition. Ethane-methane sII gas hydrates were found to have the largest shear modulus, while isobutane sII gas hydrates have the lowest. In fact, the shear properties of gas hydrates were shown to be largely influenced by the level of anisotropy in their crystal lattice, which itself is related to the size of the guest. The effect of guest size on gas hydrate properties and structure at the atomistic level has been thoroughly investigated and elucidated. The size effect can be observed not only through sII hydrate anisotropy, which increases with guest size, but also through the compressional wave velocity, which decreases with guest molecular weight. The acoustic properties of gas hydrates, such as the compressional wave velocity, are extremely important in natural gas hydrate deposit detection and concentration estimation. It was determined that the repulsive effect of the guest molecule weakens the hydrate lattice structure upon tension, but strengthens it upon compression, giving empty sII hydrates the highest tensile strength, but the lowest compressive strength, defined as

the pressure at which the lattice starts to collapse. On the other hand, isobutane sII hydrates have the lowest tensile strength, and propane-methane sII hydrates have the highest compressive strength. Furthermore, the large cages in the hydrate structure are more sensitive to changes in pressure than the small cages, and as a result are more compliant. Understanding what affects the properties and structure of gas hydrates at the molecular level is the first step towards large-scale implementation of gas hydrate applications.

For future work, it may be useful to use newer XC functionals that not only take into account van der Waals forces, but include them in the electron density calculation. In other words, a more rigorous incorporation of van der Waals interactions in the XC functional may improve the accuracy of the results, especially for empty sII gas hydrate, which has no Coulomb repulsion from the guests.

Associated Content

Supporting Information. The Supporting Information includes the equations used to calculate the polycrystalline elastic properties, an example of the energy-volume results obtained from the energy-strain analysis, and the figures presenting the results from the atomic structure analysis of the other sII gas hydrates considered in this work. This material is available free of charge via the Internet at <http://pubs.acs.org>.

Acknowledgements

This work was supported by the Natural Sciences and Engineering Research Council (NSERC), the Fonds de recherche du Québec – Nature et technologies (FRQNT), the Petroleum Research Fund, and McGill Engineering Doctoral Awards (MEDA). Computations were performed on the supercomputer Colosse from McGill University, managed by Calcul Québec and Compute Canada. The operation of this supercomputer is funded by the Canada Foundation for Innovation (CFI), ministère de l'Économie, de la Science et de l'Innovation du Québec (MESI) and FRQNT.

References

1. Englezos, P., Clathrate hydrates. *Ind. Eng. Chem. Res.* **1993**, *32*, 1251-1274.
2. Sloan Jr, E. D.; Koh, C., *Clathrate hydrates of natural gases*. CRC press: 2007.
3. Englezos, P.; Lee, J. D., Gas hydrates: A cleaner source of energy and opportunity for innovative technologies. *Korean J. Chem. Eng.* **2005**, *22*, 671-681.
4. Sloan, E. D., Fundamental principles and applications of natural gas hydrates. *Nature* **2003**, *426*, 353-363.
5. Sloan, E. D.; Koh, C. A.; Sum, A., *Natural gas hydrates in flow assurance*. Gulf Professional Publishing: 2010.
6. Stevens, J. C.; Howard, J. J.; Baldwin, B. A.; Ersland, G.; Husebø, J.; Graue, A. *Experimental hydrate formation and gas production scenarios based on CO₂ sequestration*, Proceedings of the 6th International Conference on Gas Hydrates, 2008; pp 6-10.
7. Linga, P.; Kumar, R.; Englezos, P., The clathrate hydrate process for post and pre-combustion capture of carbon dioxide. *J. Hazard. Mater.* **2007**, *149*, 625-629.
8. Mimachi, H.; Takeya, S.; Yoneyama, A.; Hyodo, K.; Takeda, T.; Gotoh, Y.; Murayama, T., Natural gas storage and transportation within gas hydrate of smaller particle: Size dependence of self-preservation phenomenon of natural gas hydrate. *Chem. Eng. Sci.* **2014**, *118*, 208-213.
9. Sultan, N.; Marsset, B.; Ker, S.; Marsset, T.; Voisset, M.; Vernant, A.-M.; Bayon, G.; Cauquil, E.; Adamy, J.; Colliat, J., Hydrate dissolution as a potential mechanism for pockmark formation in the Niger delta. *J. Geophys. Res.: Solid Earth* **2010**, *115*, B08101
10. O'Connor, F. M.; Boucher, O.; Gedney, N.; Jones, C.; Folberth, G.; Coppel, R.; Friedlingstein, P.; Collins, W.; Chappellaz, J.; Ridley, J., Possible role of wetlands, permafrost, and methane hydrates in the methane cycle under future climate change: A review. *Rev. Geophys.* **2010**, *48*, RG4005.
11. Sassen, R.; Joye, S.; Sweet, S. T.; DeFreitas, D. A.; Milkov, A. V.; MacDonald, I. R., Thermogenic gas hydrates and hydrocarbon gases in complex chemosynthetic communities, Gulf of Mexico continental slope. *Org. Geochem.* **1999**, *30*, 485-497.
12. Lu, H.; Seo, Y.-t.; Lee, J.-w.; Moudrakovski, I.; Ripmeester, J. A.; Chapman, N. R.; Coffin, R. B.; Gardner, G.; Pohlman, J., Complex gas hydrate from the Cascadia margin. *Nature* **2007**, *445*, 303-306.
13. Ecker, C.; Dvorkin, J.; Nur, A. M., Estimating the amount of gas hydrate and free gas from marine seismic data. *Geophysics* **2000**, *65*, 565-573.
14. Helgerud, M.; Waite, W. F.; Kirby, S.; Nur, A., Elastic wave speeds and moduli in polycrystalline ice Ih, sI methane hydrate, and sII methane- ethane hydrate. *J. Geophys Res.: Solid Earth* **2009**, *114*, B02212.
15. Ning, F.; Yu, Y.; Kjelstrup, S.; Vlugt, T. J.; Glavatskiy, K., Mechanical properties of clathrate hydrates: status and perspectives. *Energy Environ. Sci.* **2012**, *5*, 6779-6795.
16. Hester, K.; Huo, Z.; Ballard, A.; Koh, C.; Miller, K.; Sloan, E., Thermal expansivity for sI and sII clathrate hydrates. *J. Phys. Chem. B* **2007**, *111*, 8830-8835.
17. Rawn, C.; Rondinone, A.; Chakoumakos, B.; Circone, S.; Stern, L.; Kirby, S.; Ishii, Y., Neutron powder diffraction studies as a function of temperature of structure II hydrate formed from propane. *Can. J. Phys.* **2003**, *81*, 431-438.
18. Kieft, H.; Clouter, M.; Gagnon, R., Determination of acoustic velocities of clathrate hydrates by Brillouin spectroscopy. *J. Phys Chem.* **1985**, *89*, 3103-3108.

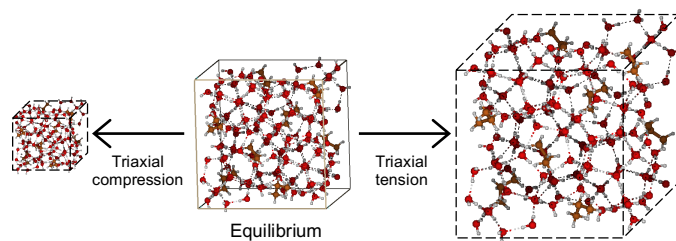
19. Stoll, R. D.; Bryan, G. M., Physical properties of sediments containing gas hydrates. *J. Geophys. Res.: Solid Earth* **1979**, *84*, 1629-1634.
20. Pandit, B.; King, M. *Elastic wave propagation in propane gas hydrates*, Proceedings of the 4th Canadian Permafrost Conference, 1982; pp 335-342.
21. Sasaki, S.; Miwa, S.; Matsuoka, T.; Kume, T., Elastic properties of methane-propane mixed gas hydrate. *Rev. High Pressure Sci. Technol.* **2014**, *24*, 270-277.
22. Huo, H.; Liu, Y.; Zheng, Z.; Zhao, J.; Jin, C.; Lv, T., Mechanical and thermal properties of methane clathrate hydrates as an alternative energy resource. *J. Renewable Sustainable Energy* **2011**, *3*, 063110.
23. Jendi, Z. M.; Rey, A. D.; Servio, P., Ab initio DFT study of structural and mechanical properties of methane and carbon dioxide hydrates. *Mol. Simul.* **2015**, *41*, 572-579.
24. Jendi, Z. M.; Servio, P.; Rey, A. D., Ideal Strength of Methane Hydrate and Ice Ih from First-principles. *Cryst. Growth Des.* **2015**, *15*, 5301-5309.
25. Jendi, Z.; Servio, P.; Rey, A., Ab initio modelling of methane hydrate thermophysical properties. *Phys. Chem. Chem. Phys.* **2016**, *18*, 10320-10328.
26. Santamaria, R.; Mondragón-Sánchez, J. A.; Bokhimi, X., Equation of State of a Model Methane Clathrate Cage. *J. Phys. Chem. A* **2012**, *116*, 3673-3680.
27. Miranda, C. R.; Matsuoka, T. *First-principles study on mechanical properties of CH₄ hydrate*, Proceedings of the 6th International Conference on Gas Hydrates, 2008.
28. Izquierdo-Ruiz, F.; Otero-De-La-Roza, A.; Contreras-García, J.; Prieto-Ballesteros, O.; Recio, J. M., Effects of the CO₂ Guest Molecule on the sI Clathrate Hydrate Structure. *Materials* **2016**, *9*, 777.
29. Zhang, Y.; Yang, W., Comment on “Generalized gradient approximation made simple”. *Phys. Rev. Lett.* **1998**, *80*, 890.
30. Vlastic, T. M.; Servio, P.; Rey, A. D., Atomistic modeling of structure II gas hydrate mechanics: Compressibility and equations of state. *AIP Adv.* **2016**, *6*, 085317.
31. Grimme, S., Density functional theory with London dispersion corrections. *Wiley Interdiscip. Rev.: Comput. Mol. Sci.* **2011**, *1*, 211-228.
32. Gillan, M. J.; Alfè, D.; Michaelides, A., Perspective: How good is DFT for water? *J. Chem. Phys.* **2016**, *144*, 130901.
33. Berland, K.; Cooper, V. R.; Lee, K.; Schröder, E.; Thonhauser, T.; Hyldgaard, P.; Lundqvist, B. I., van der Waals forces in density functional theory: a review of the vdW-DF method. *Rep. Prog. Phys.* **2015**, *78*, 066501.
34. Takeuchi, F.; Hiratsuka, M.; Ohmura, R.; Alavi, S.; Sum, A. K.; Yasuoka, K., Water proton configurations in structures I, II, and H clathrate hydrate unit cells. *J. Chem. Phys.* **2013**, *138*, 124504.
35. Falenty, A.; Hansen, T. C.; Kuhs, W. F., Formation and properties of ice XVI obtained by emptying a type sII clathrate hydrate. *Nature* **2014**, *516*, 231-233.
36. Stadler, R.; Wolf, W.; Podloucky, R.; Kresse, G.; Furthmüller, J.; Hafner, J., Ab initio calculations of the cohesive, elastic, and dynamical properties of CoSi₂ by pseudopotential and all-electron techniques. *Phys. Rev. B* **1996**, *54*, 1729.
37. Jamal, M.; Asadabadi, S. J.; Ahmad, I.; Aliabad, H. R., Elastic constants of cubic crystals. *Comput. Mater. Sci.* **2014**, *95*, 592-599.
38. Grimvall, G., *Thermophysical properties of materials*. Elsevier: 1999.
39. Shimizu, H.; Kumazaki, T.; Kume, T.; Sasaki, S., Elasticity of single-crystal methane hydrate at high pressure. *Phys. Rev. B* **2002**, *65*, 212102.

40. Shpakov, V.; Tse, J.; Tulk, C.; Kvamme, B.; Belosludov, V., Elastic moduli calculation and instability in structure I methane clathrate hydrate. *Chem. Phys. Lett.* **1998**, *282*, 107-114.
41. Jia, J.; Liang, Y.; Tsuji, T.; Murata, S.; Matsuoka, T., Elasticity and Stability of Clathrate Hydrate: Role of Guest Molecule Motions. *Sci. Rep.* **2017**, *7*, 1290.
42. Docherty, H.; Galindo, A.; Vega, C.; Sanz, E., A potential model for methane in water describing correctly the solubility of the gas and the properties of the methane hydrate. *J. Chem. Phys.* **2006**, *125*, 074510.
43. Ballard, A.; Sloan Jr, E., The next generation of hydrate prediction: I. Hydrate standard states and incorporation of spectroscopy. *Fluid Phase Equilib.* **2002**, *194*, 371-383.
44. Klapproth, A.; Goreshnik, E.; Staykova, D.; Klein, H.; Kuhs, W. F., Structural studies of gas hydrates. *Can. J. Phys.* **2003**, *81*, 503-518.
45. Kumar, P.; Sathyamurthy, N., Theoretical studies of host-guest interaction in gas hydrates. *J. Phys. Chem. A* **2011**, *115*, 14276-14281.
46. Huang, Y.; Ma, Z.; Zhang, X.; Zhou, G.; Zhou, Y.; Sun, C. Q., Hydrogen bond asymmetric local potentials in compressed ice. *J. Phys. Chem. B* **2013**, *117*, 13639-13645.
47. Huang, Y.; Zhang, X.; Ma, Z.; Zhou, Y.; Zheng, W.; Zhou, J.; Sun, C. Q., Hydrogen-bond relaxation dynamics: resolving mysteries of water ice. *Coord. Chem. Rev.* **2015**, *285*, 109-165.
48. Sikka, S., On some hydrogen bond correlations at high pressures. *High Pressure Res.* **2007**, *27*, 313-319.
49. Goryainov, S., A model of phase transitions in double-well Morse potential: Application to hydrogen bond. *Phys. B* **2012**, *407*, 4233-4237.
50. Holzapfel, W., On the symmetry of the hydrogen bonds in ice VII. *J. Chem. Phys.* **1972**, *56*, 712-715.
51. Goncharov, A. F.; Struzhkin, V. V.; Mao, H.-k.; Hemley, R. J., Raman spectroscopy of dense H₂O and the transition to symmetric hydrogen bonds. *Phys. Rev. Lett.* **1999**, *83*, 1998.
52. Chiari, G.; Ferraris, G., The water molecule in crystalline hydrates studied by neutron diffraction. *Acta Crystallogr., Sect. B: Struct. Crystallogr. Cryst. Chem.* **1982**, *38*, 2331-2341.
53. Libowitzky, E., Correlation of OH stretching frequencies and OH...O hydrogen bond lengths in minerals. *Monatsh. Chem.* **1999**, *130*, 1047-1059.
54. Kuhs, W.; Lehmann, M., The structure of the ice Ih by neutron diffraction. *J. Phys. Chem.* **1983**, *87*, 4312-4313.

For Table of Contents Use Only

Effect of Guest Size on the Mechanical Properties and Molecular Structure of Gas Hydrates from First-Principles

Thomas M. Vlastic, Phillip D. Servio, Alejandro D. Rey*



Synopsis: Density Functional Theory has been used to calculate the elastic and acoustic properties of sII gas hydrates with hydrocarbon guests. This work highlights the effect of guest size on these properties as well as on the host lattice structure at the molecular scale during triaxial compression and tension, relating microscopic characteristics to macroscopic properties.